

Corrosion Behavior of Ti-13Nb-13Zr and Ti-6Al-4V Alloys for Biomaterial Application

Viswanathan S. Saji, Yong-Hoon Jeong, Jin-Woo Yu¹, and Han-Cheol Choe[†]

Department of Dental Materials, School of Dentistry, Chosun University, Gwangju 501-759, Korea

¹Shingyeong University, 1485, Namyang-Dong, Hwaseong-Si, Gyeonggi-Do, 445-741, Korea

(Received January 7, 2010; Revised February 9, 2010; Accepted February 10, 2010)

Ti-13Nb-13Zr (TNZ) alloy has attracted considerable research attention in the last decade as a suitable substitute for the commercially used Ti-6Al-4V (TAV) alloy for orthopedic and dental implant applications. Hence, in the present work, a comparative evaluation has been performed on the electrochemical corrosion behavior of TNZ and TAV alloys in 0.9 wt.% NaCl solution. The result of the study showed that both the alloys had similar electrochemical behavior. The corrosion resistance of TAV alloy is found to be marginally superior to that of TNZ alloy.

Keywords : Ti-13Nb-13Zr, biomaterial, corrosion

1. Introduction

Titanium and titanium alloys continue to be the best choice as orthopedic and dental implant materials due to their excellent biocompatibility and mechanical properties.¹⁻⁵⁾ Among the different titanium alloys (α , $\alpha+\beta$, β), the $\alpha+\beta$ type Ti-6Al-4V (TAV) alloy is the most employed biomaterial with proven clinical success. Usually $\alpha+\beta$ microstructure of the alloy is particularly important when a greater modulus of elasticity is in need, such as bone plates. However, the release of toxic Al and V ions from the TAV alloy remains a major concern. Among the titanium alloys investigated as substitutes for TAV alloy, Ti-13Nb-13Zr (TNZ) alloy (~ 79 GPa)⁶⁾ is particularly promising and has attracted considerable recent research attention. This alloy does not contain any elemental constituents associated with adverse cell response. It has been shown that surface hardened TNZ alloy possess comparable or superior strength and toughness to existing TAV alloy.⁷⁾ The comparatively higher elastic modulus of the TAV alloy (~ 120 GPa) is unfavorable for clinical implant success, in terms of stress transmission between the implant and the bone (~ 28 GPa).⁸⁾

Corrosion is perhaps the most decisive phenomenon defining the biocompatibility and mechanical integrity of an implant. Corrosion resistance of titanium alloys depends primarily on the alloy chemical composition, alloy proc-

essing and the resulting microstructure; in addition to the texture and crystal structure.⁹⁾ Corrosion behaviors of TAV and TNZ alloy was investigated by different researchers.¹⁰⁻¹⁹⁾ Some of these reported studies suggested that corrosion resistance of TNZ alloy is superior to that of TAV alloy,^{12,16)} whereas few studies indicated a reverse trend.^{18,19)} Also, the corrosion resistance of titanium alloys varies significantly depending on the alloy processing conditions. Hence, in the present work, we have studied the corrosion behavior of TNZ and TAV alloys that were fabricated by arc melting and water quenching. The electrolyte used was de-aerated 0.9 wt.% NaCl solution at 37 ± 1 °C.

2. Experimental

The alloys have been fabricated by arc melting with non consumable tungsten electrode and water cooled copper hearth under ultra pure argon atmosphere. The ingots were re-melted 10 times in order to homogenize the alloy chemical composition. The casted alloys were heat treated at 1000 °C in Ar atmosphere, followed by water quenching. The phase structure and chemical composition of the heat treated alloys were identified by x-ray diffraction (XRD, X'pert Pro, Philips, Netherlands) using a Cu-ka radiation and energy dispersive x-ray spectroscopy (EDS, JXA-8900M, Jeol, Japan) respectively. Chemical etching was performed using Keller's reagent and the microstructure was observed by optical microscope (OM, Olympus BX 60MF, Japan). The chemical composition of the alloys as

[†] Corresponding author: hchoe@chosun.ac.kr

determined by EDS were Ti: Nb: Zr = 72.18: 13.58: 14.24 and Ti: Al: V = 89.2: 6.5: 4.3.

Electrochemical studies were conducted using a potentiostat/galvanostat (EG&G, 263A) and impedance spectroscopy (EIS, EG&G, 1025). A conventional three electrode system with high density graphite as counter electrode and saturated calomel electrode (SCE) as reference was used. The electrolyte was 0.9 wt.% NaCl at 37 ± 1 °C. The sample edges were carefully covered with epoxy to avoid the possible crevice attack. The electrolyte was de-aerated with high purity Ar gas for 30 min before starting the experiment. De-aeration was continued at a uniform rate during the experiment and the solution was subjected to mild stirring using a magnetic stirrer. The scan rate used for potentiodynamic polarization was 1.667 mV/s. An immersion period of 1 h was given for stabilization of open circuit potential (OCP) before starting the experiments. A similar three electrode set-up was used for impedance spectroscopy studies. The frequency range used for EIS studies was 10^{-2} Hz to 10^5 Hz. The amplitude of AC signal was 10 mV and 5 points per decade was used. Experiments were conducted at E_{corr} and at 300 mV.

3. Results and discussion

Representative optical micrographs of the TNZ and TAV alloy are shown in Fig. 1. Both the alloys exhibited $\alpha+\beta$ microstructure with acicular martensitic phases and intergranular β grains. XRD measurements [not shown] showed that the volume fraction of β phase in TNZ alloy is significantly higher than that of the TAV alloy. This is attributed to the higher wt.% of the Nb in the alloy, which is a β phase stabilizer. In TAV alloy, 6 wt.% Al is the α phase stabilizer and 4 wt.% V stabilizes the β phase. The comparatively higher elastic modulus of the TAV alloy is attributed to the higher volume fraction of the α phase.

Fig. 2 represents the potentiodynamic anodic polarization plots obtained for the TNZ and TAV alloys. Both the alloys exhibited steady passive region in the electrolyte, with almost similar values for the passive current density (i_{pass}), which is in the order of 10^{-6} A/cm². The potentiostatic polarization plots at 300 mV supports this result (Fig. 3). Both the alloys showed similar current density values. From the Fig. 1 & 2, it can be suggested that the corrosion resistance property of the two alloys in the present electrolyte is equivalent. However, the TNZ alloy exhibited comparatively higher passive current density values than the TAV alloy, possibly indicating enhanced passive film stability for the latter.

After the potentiostatic experiments, we have made in-

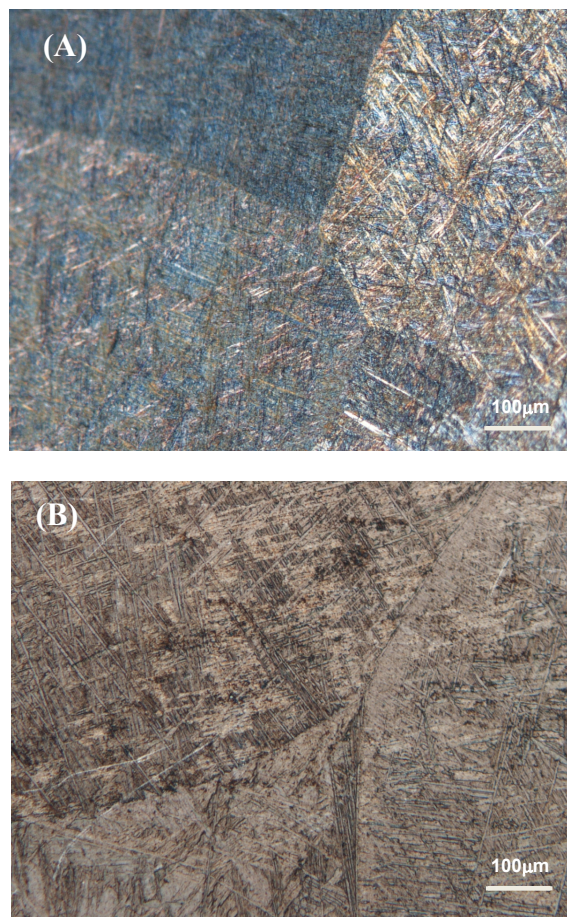


Fig. 1. Representative optical microstructures: (A) Ti-13Nb-13Zr; (B) Ti-6Al-4V.

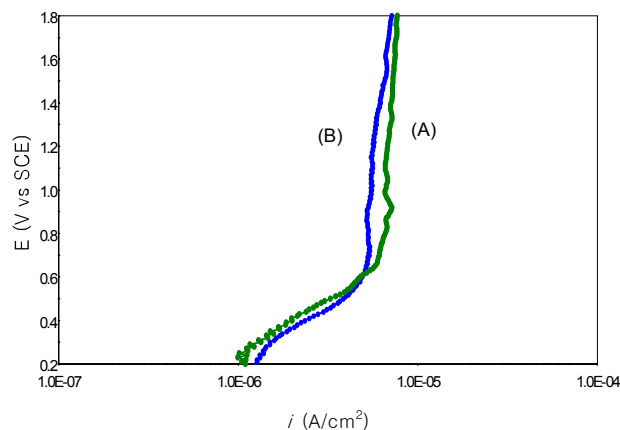


Fig. 2. Potentiodynamic anodic polarization plots: (A) Ti-13Nb-13Zr; (B) Ti-6Al-4V.

tentional scratches on the sample surface using a sharp knife edge, in order to study the ability of the passive film to repair the film damage. In actual practice, the passive layer can be broken down in certain circumstances

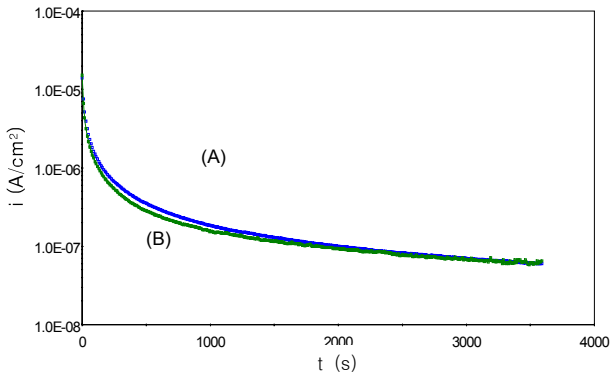


Fig. 3. Potentiostatic polarization plots recorded at 300 mV: (A) Ti-13Nb-13Zr; (B) Ti-6Al-4V.

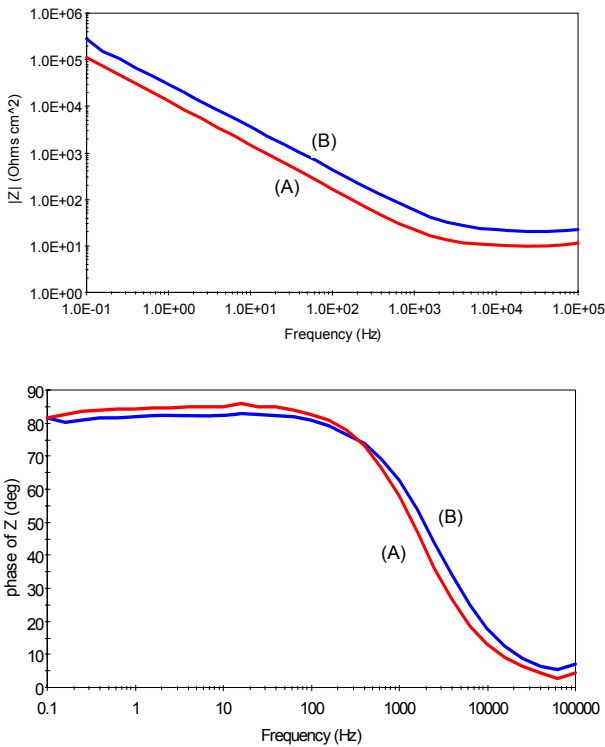


Fig. 4. Bode spectra recorded at E_{corr} : (A) Ti-13Nb-13Zr; (B) Ti-6Al-4V.

by wear. After making the surface scratches, the samples were again immersed in the same electrolyte and the variation in current density is followed as a function of applied potential at the range from 0 to 1 V. Care was taken to keep the extent of passive film damage same in both the alloys. Both the alloys exhibited similar current-voltage behavior. However, the current density values recorded for the TAV alloy was slightly nobler than that recorded for the TNZ alloy [not shown]. This observation probably suggests that the two alloys are equivalent in the film repairing ability too. This may be due to the fact that TiO_2 based

passivation is the predominant protection mechanism in both the cases. However, the performance of TAV alloy was marginally better than that of the TNZ alloy.

Fig. 4 represents the Bode plots obtained for the TNZ and TAV alloys. Collaborated with the above results, EIS plots showed higher impedance values for TAV alloy than the TNZ alloy. The phase angle was close to 90 degree for both alloys over a wide frequency range, due to the formation of thin passive oxide film. EIS measurements were also carried out at 300 Hz [not shown]. It has been showed that the passive oxide film at higher potentials is composed of an inner barrier layer and an outer porous layer.²⁰ This latter layer contains microscopic pores, whereas the barrier layer is compact and related to a very large resistance. The slight inflection observed at 1 Hz in the Bode frequency plot for both the alloys was more accentuated at 300 mV, possibly indicating two relaxation time constants. There was a considerable decrease in the phase angles at lower frequencies when compared to the corresponding plot at E_{corr} . This observation suggests deterioration of the protective properties of the passive film. Hence, an equivalent circuit corresponding to a defective coating was used for fitting the EIS graphs recorded at 300 mV.¹⁸ A simple Randle's circuit was used for fitting the graph at E_{corr} . Table 1 shows the corresponding simulated data. Here R_1 and R_2 respectively represent porous layer and barrier layer resistance. Chi-square values of the order of 10^{-3} indicated excellent agreement between the experimental and model values in both the cases. A higher value of R implies higher corrosion resistance. Hence the result of the present study indicated a marginal better performance for the TAV alloy than the TNZ alloy. However, enhanced mechanical property and biocompatibility give an advantageous edge to TNZ alloy for implant applications.

4. Conclusions

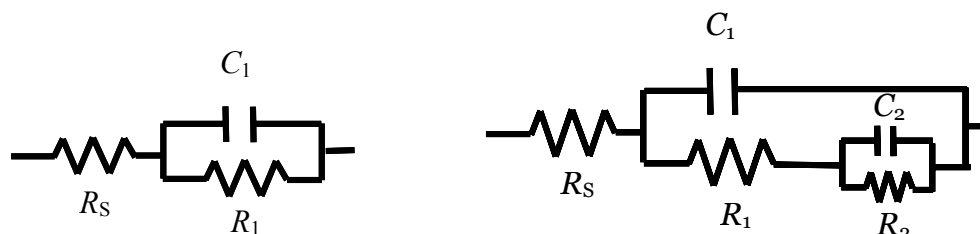
The phase and microstructure analysis showed that the beta phase fraction in the TNZ alloy is significantly higher than that in the TAV alloy. Electrochemical studies showed that both the alloys had similar electrochemical behavior in the electrolyte. The corrosion resistance of TAV alloy is slightly superior to TNZ alloy.

References

1. H.J. Rack and J.I. Qazi, *Mater. Sci. Eng.*, **C26**, 1269 (2006).
2. K. Wang, *Mater. Sci. Eng.*, **A213**, 134 (1996).
3. V.S. Saji, Y.H. Jeong, and H.C. Choe, *Corrosion Science and Technology*, **8**, 139 (2009).

Table 1. EIS simulation result

Sample		$R_s/\Omega.cm^2$	$R_1/M\Omega.cm^2$	$C_1/\mu F.cm^{-2}$	n_1	$C_2/\mu F.cm^{-2}$	$R_2/M\Omega.cm^2$	n_2
Ti-13Nb-13Zr	E_{corr}	15.16	4.47	9.48	0.94	-	-	-
	0.3 V	34.07	0.0014	7.76	0.89	2.28	6.11	0.92
Ti-6Al-4V	E_{corr}	20.37	6.04	7.17	0.92	-	-	-
	0.3 V	25.93	0.00007	6.25	0.87	1.19	8.65	0.91



4. D.Y. Kim and H.S. Kwon, *Corrosion Science and Technology*, **2**, 212 (2003).
5. M.Y. Oh, W.G. Kim, H.C. Choe, and Y.M. Ko, *Corrosion Science and Technology*, **8**, 89 (2009).
6. J.A. Davidson and P. Kovacs, US Patent 4,169,597 (1992).
7. J.A. Davidson, A.K. Mishra, P. Kovacs, and R.A. Poggie, *Biomed. Mater. Eng.*, **4**, 231 (1994).
8. D.R. Sumner and J.O. Galante, *Clin. Orthoped. Rel. Res.*, **274**, 202 (1992).
9. M. Geetha, U.K. Mudali, A.K. Gogia, R. Asokamani, and B. Raj, *Corros. Sci.*, **46**, 877 (2004).
10. S.Y. Yu and J.R. Scully, *Corrosion*, **53**, 965 (1997).
11. A. Choubey, B. Basu, and R. Balasubramaniam, *Trends Biomater Artif Organs*, **18**, 64 (2005).
12. S.L. Assis and I. Costa, *Mater Corros.*, **58**, 329 (2007).
13. S.L. Assis, S. Wolyneć, and I. Costa, *Mater. Corros.*, **59**, 739 (2008).
14. T.C. Niemeyer, C.R. Grandini, L.M.C. Pinto, A.C.D. Angelo, and S.G. Schneider, *J. Alloy. Compd.*, **476**, 172 (2009).
15. M.A. Khan, R.L. Williams, and D.F. Williams, *Biomaterials*, **20**, 631 (1999).
16. M.A. Khan, R.L. Williams, and D.F. Williams, *Biomaterials*, **17**, 2117 (1996).
17. M.F. Lo'pez, A. Gutie' rez, and J. A. Jime' nez, *Electrochim Acta*, **47**, 1359 (2002).
18. S.L. Aziz, S. Wolyneć, and I. Costa, *Electrochim Acta*, **51**, 1815 (2006).
19. Z. Cai, T. Shafer, I. Watanabe, M.E. Nunn, and T. Okabe, *Biomaterials*, **24**, 213 (2003).
20. J. Pan, D. Thierry, and C. Leygraf, *Electrochim Acta*, **41**, 1143 (1996).